

A case study about the mass exclusion limits for the BSM vector resonances with the direct couplings to the third quark generation

Mikuláš Gintner^{a,1,3}, Josef Jurán^{b,1,2}

¹Institute of Experimental and Applied Physics, Czech Technical University in Prague, Husova 240/5, 110 00 Prague, Czech Republic

²Institute of Physics, Silesian University in Opava, Bezručovo nám. 13, 746 01 Opava, Czech Republic

³Physics Department, University of Žilina, Univerzitná 1, 010 26 Žilina, Slovakia

Received: date / Accepted: date

Abstract The upper bounds that the LHC measurements searching for heavy resonances beyond the Standard model set on the resonance production cross sections are not universal. They depend on various characteristics of the resonance under consideration, like its mass, spin, and its interaction pattern. Their validity are also limited by the assumptions and approximations applied to their calculations. The bounds are typically used to derive the mass exclusion limits for the new resonances. In our work, we address some of the issues that emerge when deriving the mass exclusion limits for the strongly coupled composite $SU(2)_{L+R}$ vector resonance triplet which would interact directly to the third quark generation only. We investigate the restrictions on the applicability of the generally used limit-obtaining procedure to this particular type of vector resonances. We demonstrate that, in this case, it is necessary to consider the bottom quark partonic contents of the proton. Eventually, we find the mass exclusion limits for this resonance triplet for some representative subsets of the parameter space.

1 Introduction

The existence of new particles, complementing the established Standard model (SM) spectrum, is predicted by all major scenarios of the SM extension. Should they be the supersymmetric partners to the SM fields or the composite resonances of new strong interactions, the discovery of the new particle(s) would provide undeniable evidence for beyond the SM physics. No wonder that the search for them has its rightful place in the

ATLAS and CMS Collaboration's activities. Nevertheless, despite all their effort, no new particle has been discovered so far. Actually, not even a significant disagreement with the SM predictions has been observed yet.

Facing the absence of the positive experimental input the available data can be used to set the exclusion limits on the parameters of the candidate BSM theories. First of all, the data can be translated into the excluded values of the masses of the sought-after new particles. Indeed, both Collaborations are making an effort to process their measurements into the form that can be used to establish the mass exclusion limits for the new particles of various kinds.

Obtaining the bound and, subsequently, the mass exclusion limits for the resonance of a particular BSM theory is a challenging task that requires the contributions of the experimental as well as theoretical communities. Since there is plenty of candidate theories with new particles of different properties, both communities seek to make the procedure as simple and general as possible. However, there are principal restrictions on how model-independent the analysis can become. They result from the specific properties of the sought-after resonance, like its spin or the absence of a certain decay channel. To calculate the mass exclusion limits correctly all significant model-imposed assumptions have to be identified and taken into account properly.

In their bounds producing analyses, the ATLAS and CMS Collaborations have focused on the on-shell direct production of the new particles in the LHC proton-proton collisions. There, the resonances are searched for in their various two-particle decay channels. The absence of the statistically significant deviation from the SM prediction in a given decay channel is then be-

^ae-mail: gintner@fyzika.uniza.sk

^be-mail: josef.juran@utef.cvut.cz

ing translated into the upper bound on the production cross section of the BSM resonance multiplied by the relevant branching ratio.

In order to work out the mass exclusion limit for a particular BSM model resonance theorists have to deliver the model's cross sections that are to be compared with the experimental upper bounds for the individual channels. If such a cross section exceeds the bound the resonance (and, thus, the model) is considered as being excluded by the experiment. When the resonance mass is a free parameter of the model, the regions of the excluded mass values can be established in this way.

Any simplifications, introduced in the calculations of the model cross sections, are welcomed. However, one has to remember that the simplifying assumptions can result in the reduction of the applicability of the obtained exclusion limits.

In this paper, we study the mass exclusion limits for the strongly-interacting BSM vector resonances that could be observed at the LHC as the follow-up of the 125 GeV Higgs boson. We consider the scenario with a particular pattern of the resonance interactions with the SM fermions: the vector resonance couples directly only to the top and bottom quarks and not to any other SM fermion. This model setup is common for many strongly-interacting composite Higgs theories. In our study, we also pay attention to the impact of certain characteristic features of this scenario on the applicability of considered simplifications.

We mimic the scenario with an effective model where the Higgs sector of the effective Lagrangian is based on the non-linear sigma model with the 125-GeV $SU(2)_{L+R}$ scalar singlet complementing its non-linear triplet of the Nambu-Goldstone bosons. The vector resonances are present in the Lagrangian as an $SU(2)_{L+R}$ triplet. This setup fits the situation when the global $SU(2)_L \times SU(2)_R$ symmetry is broken down to $SU(2)_{L+R}$.

The vector triplet is introduced as a gauge field via the hidden local symmetry approach [1]. Thus, the mass eigenstate representation of the vector resonance contains the admixture of EW gauge bosons. The gauge sector of this effective description is equivalent to the gauge sector of highly-deconstructed Higgsless model with only three sites [2]. While this effective model is rather simplistic, we believe that it shares with more sophisticated theories in those features which we would like to scrutinize.

There are two specific features of the model that should be called attention to. First, the mass and decay widths of the vector resonances are entangled with the model's couplings. The vector resonance total width grows quite quickly with the resonance mass. The masses of the neutral and charged vector resonances are virtu-

ally degenerate when the resonance coupling g'' is much bigger than the $SU(2)_L \times U(1)_Y$ gauge couplings (g, g').

Secondly, as advertised above, the direct interactions of the vector triplet with the third generation quarks only are admitted in the fermion sector. These interactions grow with g'' and can be introduced as flavor and chirality dependent, with no other interactions of the vector triplet with fermions in the flavor basis¹. However, the couplings of the vector resonance to the light SM fermions emerge in the mass eigenstate basis due to the mixing of the gauge bosons. These interactions (referred to as *indirect* couplings) are universal and suppressed by $1/g''$. Thanks to the mixing-induced couplings, it is possible to produce the vector resonances also in the light-quark Drell-Yan processes at the LHC.

The experimental upper bounds, provided by the ATLAS and CMS Collaborations, are based on the narrow width resonance assumption. This assumption has its obvious benefits when deriving the experimental limits as well as for the calculation of the corresponding theoretical predictions. On the other hand, it restricts the scope of the method. It can be seen in our model. There are mass regions in the parametric space where the resonances are not so narrow and where the ratio exceeds the rule-of-thumb value of 10%. We identify the regions of the parameter space where the method can be applied to the vector triplet under consideration.

In our paper [3], we did the analysis of the exclusion limits for our effective model with no direct couplings of the vector resonance triplet to the SM fermions. The universality of the indirect couplings justified the up-down quark only approximation of the proton partonic content under which the predictions of our model were calculated.

In the present work, the question about the role of the b-quark partons in the vector boson production reappears due to the direct interactions between the vector triplet and the bottom quarks. Once more, one is tempted to ignore the tiny presence of the b-quarks in the proton, as we did in [3]. However, it will be shown that the direct couplings of the vector resonance with the bottom quark can even overwhelm the universal indirect interactions with fermions and, thus, compensate for the deficiency of the bottom quarks in the proton. In this paper, the first quark generation approximation used in [3] is upgraded to the all-sea-quark calculation.

In this paper, we establish the mass exclusion limits on the neutral and charged vector resonances of our model and observe their behavior. Because of the large dimensionality of the parameter space the full exclusion

¹Other sectors include self-interactions and the interactions with the SM EW gauge bosons and the Higgs boson.

limit analysis would be a difficult task. Therefore, we determine the exclusion limits for selected subsets of the parameter space only. The limits are based on the most recent upper bounds on the LHC production cross sections times branching ratios published by the ATLAS and CMS Collaborations. To derive the exclusion limits we inspect and use all production mechanisms and decay channels relevant to our model for which the Collaborations published the upper bounds.

This paper is organized as follows. In Section 2, our model is briefly introduced and its phenomenology concerning its decay widths and branching ratios studied. Section 3 is concerned with the calculations of the model cross sections that are to be compared with the experimental upper bounds. Section 4 contains the analysis and calculations of the exclusion mass limits for both cases of the model: without and with the direct interactions to the third quark generation. The results of our work are summarized in the Conclusions section.

2 The effective Lagrangian and its phenomenology

2.1 The boson sectors

The effective Lagrangian, we use in this paper, was studied in detail in our previous papers [4–6]. It can serve as an effective description of the LHC phenomenology of a hypothetical strongly interacting extension of the SM where the principal manifestation of this scenario would be the existence of a vector resonance triplet as a bound state of new strong interactions. The Lagrangian is built to respect the global $SU(2)_L \times SU(2)_R \times U(1)_{B-L} \times SU(2)_{HLS}$ symmetry of which the $SU(2)_L \times U(1)_Y \times SU(2)_{HLS}$ subgroup is also a local symmetry. The $SU(2)_{HLS}$ symmetry is an auxiliary gauge symmetry invoked to accommodate the $SU(2)_{L+R}$ triplet of new vector resonances. Each of the mentioned gauge groups is accompanied by its gauge coupling: g , g' , and g'' stand for $SU(2)_L$, $U(1)_Y$ and $SU(2)_{L+R}$, respectively. Beside the scalar singlet representing the 125 GeV Higgs boson and the hypothetical vector triplet, the effective Lagrangian is built out of the SM fields only. The effective Lagrangian itself can be found in [4–6].

The way the vector resonance triplet is introduced into the effective Lagrangian implies the mixing between the resonance and electroweak gauge boson fields. To decipher the physical content of the Lagrangian the gauge fields have to be transformed from the flavor to mass eigenstate basis. Note that the Greek letter ρ will denote the vector boson resonance fields in the mass eigenstate basis. Consequently, ρ^\pm and ρ^0 stand

for the charged and neutral members of the triplet, respectively.

When $g'' \gg g, g'$ the masses of the charged and neutral vector resonances are virtually degenerate. The leading order formula for the vector resonance mass reads

$$M_\rho = \sqrt{\alpha} g'' v / 2, \quad (1)$$

where α is a dimensionless free parameter emerging in the effective Lagrangian and v is the electroweak symmetry breaking scale. Usually, α is traded off for M_ρ so that the latter can serve as one of the free parameters of the model. Our previous studies of the low-energy limits [4, 5] as well as the Higgs-related limits and the unitarity limits [6] suggest that we should consider $M_\rho \geq 1$ TeV and $12 \leq g'' \leq 25$. Following the conventions used in the formulation of our Lagrangian the naive perturbativity bound on g'' reads $g''/2 \leq 4\pi$.

In this paper, we calculate processes with the direct production of the vector resonances followed by their two-particle decays. In the boson sector, the contributing triple couplings of the model include ρWW and ρWZ triple interactions. Their strengths are proportional to $1/g''$. Note that the model contains neither of the ρZZ , $\rho Z\gamma$, $\rho\gamma\gamma$, and $\rho W\gamma$ vertices.

Additional bosonic triple vertices that could play a role in setting the mass exclusion limits include the ρWH and ρZH vertices. Both couplings are proportional to the $a_V - a_\rho$ difference and they are also suppressed by the factor $1/g''$. To a high precision, a_V can be considered as a free pre-factor of the HWW and HZZ vertices. The $H\rho^0\rho^0$ and $H\rho^+\rho^-$ couplings are virtually proportional to a_ρ . The corresponding interaction Lagrangian, along with the calculations of the LHC experimental limits for a_V and a_ρ , can be found in [6].

Throughout this paper, we set $a_V = 1$ (the SM case) and $a_\rho = 0$ (no Higgs-to-vector resonance coupling). These values are consistent with the experimentally preferred points of the parameter space [6]. This choice that zeros the $H\rho^0\rho^0$ and $H\rho^+\rho^-$ vertices and sets the HWW and HZZ vertices to their SM form has no impact on our analysis. Neither it affects the results through the ρWH and ρZH vertices.

To the leading order in g'' the vector resonance partial decay widths to W^+W^- and $W^\pm Z$ read

$$\Gamma_{\rho \rightarrow V_1 V_2} = \Gamma_\rho \cdot [1 + 7(x_1^2 + x_2^2) - 26(x_1^4 + x_2^4) - 50x_1^2 x_2^2 + \mathcal{O}(x^6)], \quad (2)$$

where

$$\Gamma_\rho = \frac{M_\rho}{48\pi g''^2} \left(\frac{M_\rho}{v} \right)^4, \quad (3)$$

$x_{1,2} = M_{1,2}/M_\rho$, and V_i stands for either W or Z .

The partial decay widths to the WH and WZ channels read

$$\Gamma_{\rho^\pm \rightarrow W^\pm H} = 4\Gamma_\rho \cdot (a_\rho - a_V)^2 [x_W^4 + \mathcal{O}(x^6)], \quad (4)$$

and

$$\Gamma_{\rho^0 \rightarrow ZH} = 4\Gamma_\rho \cdot (a_\rho - a_V)^2 [(2x_W^2 - x_Z^2)^2 + \mathcal{O}(x^6)] \quad (5)$$

respectively. Within the 1 – 3 TeV mass interval, the WH and WZ decay widths are four to six orders of magnitude smaller than the W^+W^- and $W^\pm Z$ ones.

If there are no direct interactions of the vector resonance with fermions in the model, the widths of the fermion-related decay channels of the vector resonance are also quite negligible when compared to the W^+W^- and $W^\pm Z$ decay channels. Thus, the total decay widths of the vector resonances, both neutral and charged, can be well approximated by the expression (3).

In Fig. 1, we depict how the vector resonance total width depends on the resonance mass and g'' using the full tree-level formulas for the calculations. The dashed lines correspond to the no-direct-interaction total widths when $g'' = 12, 18$, and 24 , respectively. There is no visible distinction between the neutral and charged resonance curves in this graph. Different shadings of the background indicate regions with different values of the fatness of the resonance, $\Gamma_{\text{tot}}/M_\rho$. The graph also shows how the total width responds to the direct interactions. However, this part will be discussed in the following subsection.

2.2 The fermion sector

The only fermions considered in our effective model are those of the SM. Thus, the model describes the BSM situation when either non-SM fermionic fields are much heavier than $\mathcal{O}(1)$ TeV vector resonances or their interactions make their existence irrelevant to our analysis.

Even if no direct couplings of the vector resonance fields to fermions are introduced in the flavor eigenstate basis the mixing between the vector resonance triplet and the electroweak gauge bosons induces the couplings between the vector resonance and fermions. These “in-direct” couplings are proportional to $1/g''$.

Nevertheless, the considered symmetry also admits the introduction of the direct interactions of the vector resonance with fermions. In fact, having grouped the right fermion fields into $SU(2)_R$ doublets the considered global symmetry of the model also allows for assigning different direct couplings to each of the $SU(2)_L$ and $SU(2)_R$ fermion doublets.

We assume in our model that the flavor basis vector triplet couples directly to the quarks of the third generation only and to none of the other SM fermions. This

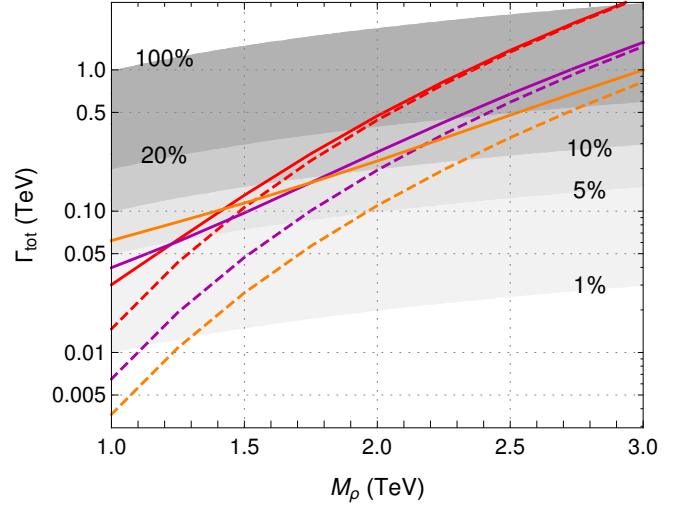


Fig. 1 The total decay width of the vector resonance as a function of the resonance mass. Top to bottom, the dashed lines correspond to $g'' = 12, 18$, and 24 , respectively, when there is no direct interaction of the vector resonance to fermions. The solid lines representing the case of the direct interactions with $b_{L,R} = -0.1$, and $p = 1$ unite with their dashed g'' -counterparts at the upper right corner of the graph. Different shadings of the background indicate areas with different value ranges of $\Gamma_{\text{tot}}/M_\rho$. The curves do not distinguish between neutral and charged resonances.

assumption is motivated by the anticipated extraordinary role of the top quark (and, perhaps, bottom quark as well) in new physics related to strong electroweak symmetry breaking. Similar interaction patterns can be found in various strong extensions of the SM including the partial compositeness and extra-dimensional scenarios. In our model, the free pre-factors for the couplings to the left and right top-bottom quark doublets are referred to as b_L and b_R , respectively [4].

In the mass basis, the direct interactions also contaminate the couplings of W and Z to the top and bottom quarks. The contamination is proportional to $b_{L,R}$. It results in the experimental restrictions on $b_{L,R}$ from the EW precision measurements [5].

In the most general case of our model, an additional free pre-factor p is introduced which serves to further modify the direct coupling to the right bottom quark. Assuming $0 \leq p \leq 1$, the p parameter can be used to suppress the direct coupling to the right bottom quark relative to the direct coupling to the right top quark; $p = 1$ leaves both interactions equal, $p = 0$ turns off the right bottom quark interaction completely and maximally breaks the $SU(2)_R$ part of the Lagrangian symmetry down to $U(1)_{R3}$. Recall that the $SU(2)_R$ symmetry is broken by the weak hypercharge interactions anyway and, thus, the $SU(2)_R$ fermion doublets are not well justified once the global symmetry gets gauged anyway.

This effective model was introduced and investigated in [4–6] as a modification of the so-called BESS model [7]. We refer to our model as the “top-BESS model” (tBESS) in order to recall its relation to its predecessor as well as to stress the special role of the top quark (or the third quark generation) in it. As was shown in [4, 5], these modifications also help relax some experimental restrictions burdening the original BESS model. Should we briefly summarize the conclusions reached in these studies, the absolute values of $b_{L,R}$ should not exceed 0.1, roughly speaking. As far as p is concerned, its most preferred value lies in the 0.2 – 0.3 interval. However, the statistical preference of the interval with respect to any other value of p between zero and one is weak.

Assuming massless fermions in the final state, the partial decay widths of the neutral vector resonance to the leptonic $\nu\nu$ and $\ell\ell$ channels read

$$\Gamma_{\rho^0 \rightarrow \nu\nu} = 8\Gamma_\rho \cdot (2x_W^2 - x_Z^2)^2, \quad (6)$$

and

$$\Gamma_{\rho^0 \rightarrow \ell\ell} = 8\Gamma_\rho \cdot [x_Z^4 + 4(x_Z^2 - x_W^2)^2], \quad (7)$$

respectively. Its partial decay widths to the light quark channels are

$$\Gamma_{\rho^0 \rightarrow uu} = 24\Gamma_\rho \cdot \frac{17x_Z^4 + 20x_W^4 - 28x_Z^2x_W^2}{9}, \quad (8)$$

and

$$\Gamma_{\rho^0 \rightarrow dd} = 24\Gamma_\rho \cdot \frac{5x_Z^4 + 20x_W^4 - 16x_Z^2x_W^2}{9}, \quad (9)$$

respectively. The corresponding partial decay widths of the charged vector resonance read

$$3\Gamma_{\rho^\pm \rightarrow \nu\ell} = \Gamma_{\rho^\pm \rightarrow ud} = 48\Gamma_\rho \cdot x_W^4. \quad (10)$$

The partial widths of the decay channels with the top and bottom quarks in the final state are sensitive to the free parameters $b_{L,R}$ and p . They originate from the intertwining of the direct and indirect interactions. The tt partial width reads

$$\Gamma_{\rho^0 \rightarrow tt} = \frac{M_\rho}{8\pi} \beta_t \{ [(g_{\rho tt}^L)^2 + (g_{\rho tt}^R)^2] (1 - x_t^2) + 6g_{\rho tt}^L g_{\rho tt}^R x_t^2 \}, \quad (11)$$

where $\beta_t = \sqrt{1 - 4x_t^2}$, $x_t = M_t/m_\rho$, and

$$g_{\rho tt}^L = -\frac{b_L}{4}g'' + \frac{2}{g''} \left[\left(\frac{2}{3} - b_L \right) \frac{M_W^2}{v^2} + \frac{1}{3} \frac{M_Z^2}{v^2} \right], \quad (12)$$

$$g_{\rho tt}^R = -\frac{b_R}{4}g'' + \frac{2}{g''} \left(\frac{4}{3} - b_R \right) \left(\frac{M_Z^2}{v^2} - \frac{M_W^2}{v^2} \right). \quad (13)$$

To the leading order in g'' , the partial width (11) reads

$$\Gamma_{\rho^0 \rightarrow tt} = \frac{3}{8}\Gamma_\rho \cdot g''^4 [(b_L^2 + b_R^2) x_v^4 + \mathcal{O}(x^6)], \quad (14)$$

where $x_v = v/M_\rho$ and $\mathcal{O}(x^6)$ represents any terms proportional to $x_v^m x_t^n x_W^p x_Z^q$ such that $m + n + p + q \geq 6$.

When the bottom mass is neglected the bb partial width reads

$$\Gamma_{\rho^0 \rightarrow bb} = \frac{M_\rho}{8\pi} [(g_{\rho bb}^L)^2 + (g_{\rho bb}^R)^2], \quad (15)$$

where

$$g_{\rho bb}^L = \frac{b_L}{4}g'' + \frac{2}{g''} \left[\left(b_L - \frac{4}{3} \right) \frac{M_W^2}{v^2} + \frac{1}{3} \frac{M_Z^2}{v^2} \right], \quad (16)$$

$$g_{\rho bb}^R = p^2 \frac{b_R}{4}g'' + \frac{2}{g''} \left(p^2 b_R - \frac{2}{3} \right) \left(\frac{M_Z^2}{v^2} - \frac{M_W^2}{v^2} \right). \quad (17)$$

To the leading order in g'' , the partial width (15) reads

$$\Gamma_{\rho^0 \rightarrow bb} = \frac{3}{8}\Gamma_\rho \cdot g''^4 (b_L^2 + p^4 b_R^2) x_v^4. \quad (18)$$

Since we ignore the bottom quark mass there are no higher order corrections above $\mathcal{O}(x^4)$ to this expression.

Finally, the tb partial width is

$$\Gamma_{\rho^\pm \rightarrow tb} = \frac{M_\rho}{8\pi} [(g_{\rho tb}^L)^2 + (g_{\rho tb}^R)^2] (1 - 3x_t^2/2 + x_t^6/2), \quad (19)$$

where

$$g_{\rho tb}^L = -\frac{b_L}{2\sqrt{2}}g'' + \frac{2\sqrt{2}}{g''} (1 - b_L) \frac{M_W^2}{v^2}, \quad (20)$$

$$g_{\rho tb}^R = -p \frac{b_R}{2\sqrt{2}}g''. \quad (21)$$

To the leading order in g'' , the partial width (19) reads

$$\Gamma_{\rho^\pm \rightarrow tb} = \frac{3}{4}\Gamma_\rho \cdot g''^4 [(b_L^2 + p^2 b_R^2) x_v^4 + \mathcal{O}(x^6)]. \quad (22)$$

2.3 The branching ratios

If the vector resonance triplet does not interact with the fermions directly ($b_{L,R} = 0$), the branching ratios of all decay channels under consideration do not depend on g'' . This is because all relevant decay widths are proportional to $(1/g'')^2$. The no direct interaction branching ratios of the neutral as well as charged vector resonances are plotted in Fig. 2. The upper graph depicts curves for $\rho^0 \rightarrow W^+W^-$, $t\bar{t}$, and $b\bar{b}$. The lower graph shows the curves for the $\rho^+ \rightarrow W^+Z$ and $t\bar{b}$ channels. In addition, the upper and lower graphs contain plots of $\delta\Gamma_0/\Gamma_{\text{tot}}^{(0)}$ and $\delta\Gamma_+/ \Gamma_{\text{tot}}^{(+)}$, respectively, where

$$\delta\Gamma_0 = \Gamma_{ZH} + 3\Gamma_{\nu\nu} + 3\Gamma_{\ell\ell} + 2\Gamma_{uu} + 2\Gamma_{dd}, \quad (23)$$

$$\delta\Gamma_+ = \Gamma_{WH} + 3\Gamma_{\nu\ell} + 2\Gamma_{ud}, \quad (24)$$

and

$$\Gamma_{\text{tot}}^{(0)} = \Gamma_{WW} + \Gamma_{tt}(b_L, b_R) + \Gamma_{bb}(b_L, p^2 b_R) + \delta\Gamma_0, \quad (25)$$

$$\Gamma_{\text{tot}}^{(+)} = \Gamma_{WZ} + \Gamma_{tb}(b_L, p b_R) + \delta\Gamma_+, \quad (26)$$

where we have assumed the same decay widths for the corresponding decay channels across all generations of

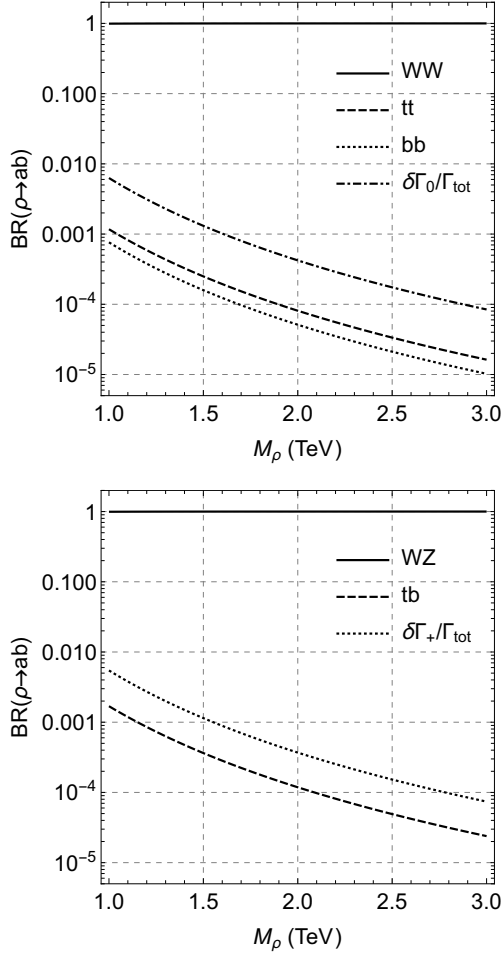


Fig. 2 The branching ratios of the neutral (top) and charged (bottom) vector resonances as functions of the resonance mass when there are no direct interactions of the resonance triplet with the top and bottom quarks.

leptons as well as across the first two generations of quarks. The CKM matrix is set to unity throughout the paper.

Now, let us consider the situation when the vector resonance triplet interacts directly with the third quark generation. It means that some or all of the b_L, b_R, p parameters assume non-zero values. The five parameters of interest that can be varied independently, M_ρ , g'' , and b_L, b_R, p , are too many for displaying the BR's behavior in a single plot. However, it is instructive to show BR's for the neutral and charged resonances as functions of their direct interactions to fermions when $b_L = b_R \equiv b_{L=R}$ and for a specific choice of the values of other parameters. Namely, we choose $M_\rho = 1$ TeV, $g'' = 18$ and $p = 0.75$. The corresponding graph can be found in Fig. 3.

As expected, the Fig. 3 behavior of the branching ratios in the vicinity of $b_L = b_R = 0$ corresponds well to that observed in Fig. 2. When $|b_{L=R}| \lesssim 10^{-2}$ the vector

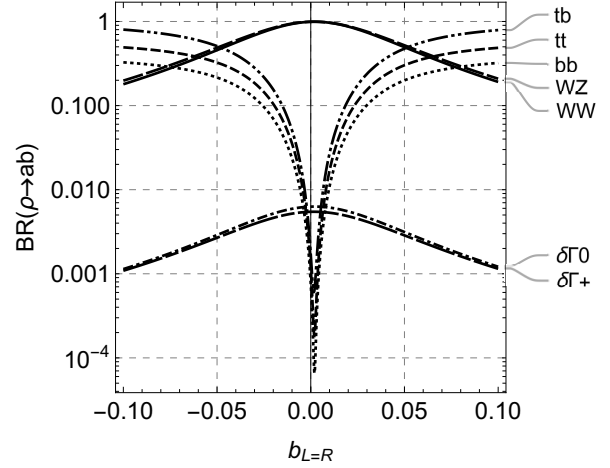


Fig. 3 The branching ratios of the neutral and charged vector resonances as functions of $b_{L=R} \equiv b_L = b_R$ when $M_\rho = 1$ TeV, $g'' = 18$ and $p = 0.75$. The labels $\delta\Gamma_0$ and $\delta\Gamma_+$ indicate the branching ratios corresponding to the decay widths given in the Eqs. (23) and (24), respectively.

resonance decays are strongly dominated by the vector boson channels. The remaining channels contribute less than 1% to the total decay widths. In addition, in this region, the combined effect of the direct and indirect interactions of the vector resonance with the top and bottom quarks pulls the branching ratios of $\rho \rightarrow tt, bb, tb$ even below those of the light fermions. Actually, there are non-zero values of $b_{L,R}$ for which the direct and indirect interactions cancel each other out and the vector resonances cease to decay to² tt, bb , and tb . The glimpse of this effect can be seen in Fig. 3 where the minimum of the tt, bb, tb curves is shifted slightly to the right of $b_{L=R} = 0$, namely at about $b_{L=R} = 0.002$.

The branching ratios of the tt, bb , and tb channels grow fast with the increasing $|b_{L=R}|$. It results from the unleashing the large contributions of the first terms of the couplings (12), (13), (16), (17), (20), and (21). These branching ratios reach the branching ratios of the light fermion channels at about $|b_{L,R}| \approx 0.01$ and they become comparable with the gauge boson ratios at about $|b_{L,R}| \approx 0.05$. Of course, the exact numbers depend on the values of the model parameters. Fig. 3 just illustrates this model's behavior.

As the direct interactions grow stronger, the branching ratios of the tt, bb , and tb channels become dependent on the g''/M_ρ ratio only. This can be seen in the leading-order-in- g'' formulas for tt, bb , and tb channels when $x_a = M_a/M_\rho = 0$ for all relevant final state par-

² The effect of the cancellation was studied in detail in our paper [4]. We nicknamed the parameter space region where the negative interference of the direct and indirect interactions suppressed the productions of $t\bar{t}, b\bar{b}$, and $t\bar{b}/b\bar{t}$ as “the Death Valley”.

ticles. These approximations introduce deviations from the exact branching ratios at the level of $x_{W,Z,t}^2$ and higher in the leading-order-in- g'' terms. The branching ratios of the principal decay channels in this approximation are displayed in Fig. 4 (the neutral resonance) and Fig. 5 (the charged resonance).

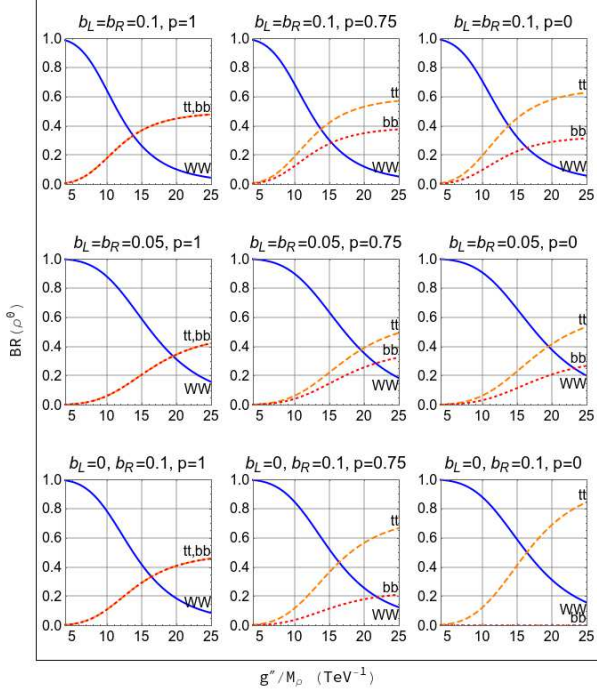


Fig. 4 The principal branching ratios of the neutral vector resonance as functions of g''/M_ρ in the approximation of the leading order in g'' and $x_a = M_a/m_\rho = 0$ where $a = W, Z, t$. The blue solid line stands for the WW channel, the orange dashed line for the tt channel and the red dotted line represents the bb channel.

Nevertheless, the calculations of the mass exclusion limits in this paper are performed using the exact expressions for the decay widths and branching ratios. The approximations discussed above are meant to provide a better insight into the analysis and a better understanding of the results.

3 Cross section calculations

In principle, the current exclusion limits on the masses of new resonances result from the comparison of the upper experimental bounds for the resonance s -channel production cross sections to the model's predictions for this observable. The upper bounds are calculated by the ATLAS and CMS Collaborations using their data for various final states of various decay channels of the vector resonances. Consequently, the provided upper bounds restrict the on-shell cross sections $\sigma(pp \rightarrow$

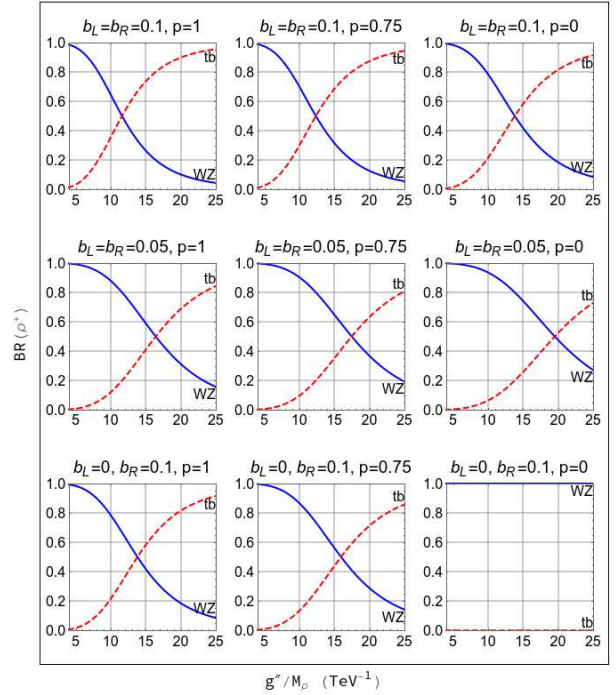


Fig. 5 The principal branching ratios of the charged vector resonance as functions of g''/M_ρ in the approximation of the leading order in g'' and $x_a = M_a/m_\rho = 0$ where $a = W, Z, t$. The blue solid line stands for the WZ channel and the red dashed line represents the tb channel.

$\rho X \rightarrow abX$). Of course, the assumptions and procedures used in the model's prediction calculations have to comply with those used by the Collaborations in obtaining the upper bounds.

As long as the decay width of the produced resonance is not too wide for its mass, the cross section $\sigma(pp \rightarrow \rho X \rightarrow abX)$ can be conveniently approximated by the Narrow Width Approximation (NWA) formula

$$\sigma(pp \rightarrow abX) = \sigma_{\text{prod}}(pp \rightarrow \rho X) \times \text{BR}(\rho \rightarrow ab), \quad (27)$$

where σ_{prod} is the on-shell cross section for the vector resonance production, and $\text{BR}(\rho \rightarrow ab)$ is the branching ratio for the vector resonance decay channel $\rho \rightarrow ab$. It is generally expected that the approximation (27) works well when $\Gamma_{\text{tot}}/M_\rho \lesssim 10\%$. One should also remember that the NWA ignores the signal-background interference effects. The influence of these effects on the precision of the approximation have been inspected in [8].

The experimental upper bounds have been delivered and updated continually by both Collaborations as, over the recent years, the amount of the data collected grew and no signs of new particles emerged. The collaborations worked out and published the upper bounds not only for the individual decay channels but also for their combinations. In addition, for the WW and WZ channels, they were able to distinguish between

the Drell-Yan (DY) and Vector Boson Fusion (VBF) production mechanisms. While, in the former case, the vector resonance is produced via the annihilation of the quarks of the colliding protons, in the latter, the resonance is created via the fusion of the electroweak vector bosons emitted by the colliding protons.

In our calculations, $\sigma(pp \rightarrow abX)$ is approximated by the sum of the DY and VBF cross sections³. We ignore the top quark involvement in the vector resonance production and approximate the CKM matrix by the unity. On the other hand, we demonstrate in this Section that the bottom quark contribution to the production cannot be neglected. Therefore, the DY production of our triplet resonance can proceed only via $u\bar{u}, d\bar{d}, c\bar{c}, s\bar{s}, b\bar{b} \rightarrow \rho^0$, and $u\bar{d}, c\bar{s} \rightarrow \rho^+$ (+c.c.).

In the VBF production, the vector resonance can emerge from $W^+W^- \rightarrow \rho^0$ and $W^+Z \rightarrow \rho^+$ (+c.c.). This production is calculated in the Effective-W Approximation (EWA) [9] considering the longitudinal W/Z degrees of freedom only.

3.1 Production cross section

The first factor in the calculation of the cross section (27) for the given decay channel is the production cross section $\sigma_{\text{prod}}(pp \rightarrow \rho X)$. We address its calculation in this Subsection. The production cross section of a resonance can be expressed as

$$\sigma_{\text{prod}}(pp \rightarrow \rho X) = \sum_{A \leq B} 16\pi^2 K_{AB} F_{AB} \frac{d\Pi_{AB}}{d\hat{s}}|_{\hat{s}=M_\rho^2}, \quad (28)$$

where $F_{AB} = \Gamma_{\rho \rightarrow AB}/M_\rho$ and $\Gamma_{\rho \rightarrow AB}$ are, respectively, the partial fatness and the partial decay width of the resonance to the partons A and B of the colliding protons. Furthermore, $d\Pi_{AB}/d\hat{s}$ is the differential luminosity of the colliding partons, and

$$K_{AB} = \frac{2J+1}{(2S_A+1)(2S_B+1)} \frac{C}{C_A C_B}, \quad (29)$$

where J is the spin of the resonance, C is its color factor, and S_A, S_B and C_A, C_B are the spins and colors of the initial partons, respectively⁴. In this paragraph, by ‘‘partons’’ we also refer to the electroweak gauge bosons emitted of the partonic quarks of the colliding protons in the case of the VBF production.

Note that the model dependence can enter the production cross section (28) only via the partial decay widths $\Gamma_{\rho \rightarrow AB}$. The concerned widths include $\Gamma_{uu}, \Gamma_{dd},$

³The gluon-gluon production via loops is excluded by the Landau-Yang theorem.

⁴The tBESS vector resonance values: $J_\rho = 1$, $C_\rho = 1$, $S_q = 1/2$, $C_q = 3$, $J_{W_L, Z_L} = 0$, $C_{W_L, Z_L} = 1$. Consequently, $K_{qq'} = 1/12$, $K_{W_L W_L} = K_{W_L Z_L} = 3$.

$\Gamma_{cc}, \Gamma_{ss}, \Gamma_{ud}, \Gamma_{cs}, \Gamma_{bb}, \Gamma_{WW}$ and Γ_{WZ} where $\Gamma_{uu} = \Gamma_{cc}$, $\Gamma_{dd} = \Gamma_{ss}$, $\Gamma_{ud} = \Gamma_{cs}$. In the VBF production processes, all F_{AB} ’s are proportional to M_ρ^4/g'^2 up to some small corrections of higher order. All DY partial fatnesses F_{AB} , but the F_{bb} one, are proportional to $1/g'^2$ and do not depend on M_ρ . The bb channel is the only one through which the production cross section is sensitive to the couplings of the direct interactions. If the direct couplings are sufficiently large then F_{bb} is virtually proportional to $g'^2(b_L^2 + p^4 b_R^2)$. Neither this fatness depends on M_ρ .

The production cross section (28) also depends on the parton contents of the proton via the differential parton luminosities $d\Pi_{AB}/d\hat{s}$, or ‘‘quasi-luminosities’’ for short. In the DY process, the quasi-luminosities for various partons are obtained from the standard formula

$$\frac{d\Pi_{AB}}{d\hat{s}} = \frac{1}{s} \int_\tau^1 \frac{dx}{x} \frac{1}{1 + \delta_{AB}} [f_A(x, \hat{s}) f_B(\tau/x, \hat{s}) + A \leftrightarrow B], \quad (30)$$

where s and \hat{s} are the squared center of mass energies of the colliding protons and quarks, respectively, $f_A(x)$ is a p.d.f. of the quark A with the momentum fraction x of its proton’s momentum, and $\tau = \hat{s}/s$. The formula for the quasi-luminosity in the VBF production reads

$$\frac{d\Pi_{AB}}{d\tau} = \sum_{i \leq j} \frac{1}{1 + \delta_{ij}} \int_\tau^1 \frac{dx_1}{x_1} \int_{\tau/x_1}^1 \frac{dx_2}{x_2} [f_i(x_1, q^2) f_j(x_2, q^2) \frac{dL_{A[i]B[j]}}{d\hat{\tau}} + i \leftrightarrow j], \quad (31)$$

where $\hat{\tau} = \tau/(x_1 x_2)$, and $dL_{A[i]B[j]}/d\hat{\tau}$ is the luminosity for two vector bosons A and B emitted from i th and j th quarks, respectively.

The vector boson luminosity $dL_{A[i]B[j]}/d\hat{\tau}$ is calculated using the EWA method. This approach is also a subject to some assumptions and restrictions. First of all, the gauge bosons are assumed to be emitted on-shell and in small angles to their parental quarks. Secondly, the masses of the fusing gauge bosons should be much smaller than the produced resonance mass. Finally, the transversal and longitudinal polarizations of the emitted gauge bosons are to be considered as separate modes.

In the presence of the deviations from the SM, the longitudinal mode usually dominates. Therefore, in our calculations, we consider contributions from this mode only. The EWA luminosity for two longitudinal vector bosons A and B emitted from i th and j th quarks reads

$$\frac{dL_{A[i]L B[j]L}}{d\hat{\tau}} = \frac{v_{A[i]}^2 + a_{A[i]}^2}{4\pi^2} \frac{v_{B[j]}^2 + a_{B[j]}^2}{4\pi^2} \frac{1}{\hat{\tau}} [(1 + \hat{\tau}) \log(1/\hat{\tau}) - 2(1 - \hat{\tau})], \quad (32)$$

where $v_{A[i]}$ and $a_{A[i]}$ are the vector and axial-vector couplings of the electroweak gauge boson A to the quark current of q_i , respectively.

In Fig. 6, the quasi-luminosities for the DY and VBF LHC processes at $\sqrt{s} = 13$ TeV are shown. For the numerical evaluation the `Mathematica` package `ManeParse` [10] with the CT10 p.d.f. set from the LHAPDF 6 library in the HepForge repository [11] is used. As can

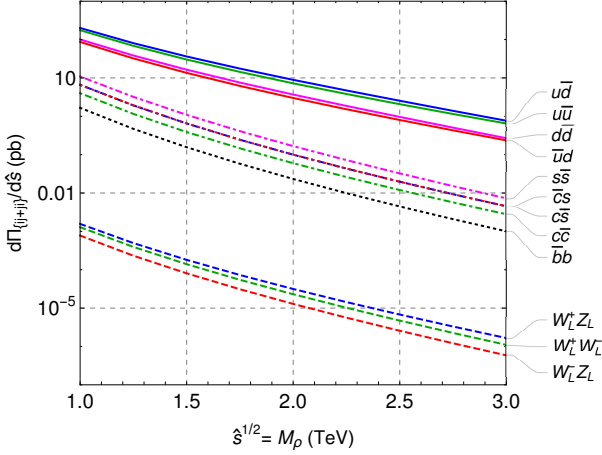


Fig. 6 Quasi-luminosities for the DY and VBF LHC processes at $\sqrt{s} = 13$ TeV as functions of the CMS energy of the colliding partons.

be seen, the DY quasi-luminosities dominate by many orders of magnitude over the quasi-luminosities of the VBF production. It is because the VBF production process is suppressed against the DY production process by two orders in the perturbative expansion.

The relative sizes of the individual DY quasi-luminosities can be understood in terms of the proton parton contents for individual flavors. The valence quark quasi-luminosities clearly stand over the sea quark ones. The bb quasi-luminosity is the smallest one by 2 – 3 orders of magnitude below the u and d related quasi-luminosities. This poses a question whether the contribution of the vector resonance production via the sea quark annihilation are worthy of consideration. Of these, the $b\bar{b} \rightarrow \rho^0$ production is the most disputable. On the one hand, the $b\bar{b}$ quasi-luminosity contributes the least. On the other hand, this is the only production process that is sensitive to the direct interactions.

To address this issue the production cross section (28) is plotted as a function of the resonance mass for the DY and VBF modes assuming $g'' = 20$. In the DY case, we also distinguish between the situations with and without the direct interactions. However, only the neutral resonance DY production is sensitive to the direct interactions. Therefore, turning the direct interactions on by setting $b_L = b_R = 0.1$, $p = 1$ affects only the neutral

DY mode. All these plots are shown in Fig. 7. The plotted production cross sections are calculated considering contributions of all quark flavors but the top quark to the proton partonic contents.

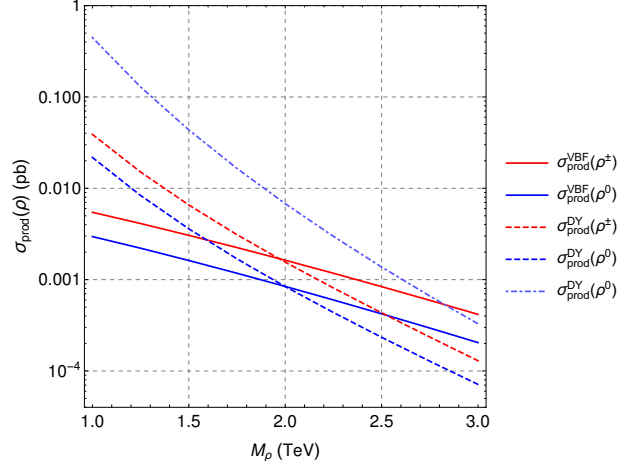


Fig. 7 The production cross sections $\sigma_{\text{prod}}(pp \rightarrow \rho X)$ for the DY and VBF productions of the neutral (blue) and charged (red) vector resonances as functions of the resonance mass when $g'' = 20$. The solid lines stand for the VBF production which is insensitive to the direct interactions. The dashed lines denote the DY production without the direct interactions. The dot-dashed line shows the neutral DY case with the direct interactions, namely $b_L = b_R = 0.1$, $p = 1$.

The following observations can be made in Fig. 7. First of all, in spite of much smaller quasi-luminosity, the VBF production cross section is comparable with the DY one. It is because the VBF production quasi-luminosity handicap is counter-balanced with the dominance of $F_{WW,WZ}$ over F_{qq} (see Figs. 2 and 3). Therefore, both production modes must be considered in our analysis. The different slopes of the DY and VBF curves can be understood when we recall that $F_{qq} \propto M_\rho^0$ while $F_{WW,WZ} \propto M_\rho^4$.

Secondly, we can see that the direct interactions can have a visible impact on the production cross section for the neutral DY mode. When $M_\rho = 1$ TeV and $g'' = 20$ the contributions of $b\bar{b} \rightarrow \rho^0$ to the production cross section is 12% and 95% when $b_L = b_R = 0.01$, $p = 1$ and $b_L = b_R = 0.1$, $p = 1$, respectively.

Since the sea-without- b quark production of the vector triplet is not sensitive to the direct interactions, it is reasonable to expect that its contribution to the production cross section will be small under all circumstances. The size of this contribution cannot be read off of Fig. 7. In our calculations, we have established that by ignoring the sea quark production in the no-direct-interaction situation the production cross section is lowered by about 7% when $M_\rho = 1$ TeV and by about

5% at $M_\rho = 3$ TeV. The discrepancy decreases as M_ρ grows.

3.2 $\sigma_{\text{prod}} \times \text{BR}$

Following Eq. (27), $\sigma(pp \rightarrow \rho X \rightarrow abX)$ is obtained when the production cross section is multiplied by the branching ratio of $\rho \rightarrow ab$. When there are no direct interactions of the vector triplet with top and bottom quarks more than 99% of ρ decays into the WW/WZ channel. It can be seen in Fig 2. To a high accuracy, this assertion holds for any considered values of g'' and M_ρ . Therefore, $\sigma_{\text{prod}} \times \text{BR}(\rho \rightarrow WW/WZ)$ is virtually identical with the production cross section σ_{prod} .

The direct interactions influence the resulting cross sections solely via the branching ratios with a single exception. The exception is the neutral resonance production via the DY mode. There, the production depends on the parameters of the direct interactions as well. Recall that the dependence originate in the $b\bar{b} \rightarrow \rho^0$ vertex.

The direct interactions can alter the vector resonance branching ratios of the individual channels significantly. It can be inferred from the behavior of $\text{BR}(\rho \rightarrow WW/WZ)$ and $\text{BR}(\rho \rightarrow tt/bb/tb)$ as it is depicted in Figs. 3, 4, and 5. The prevailing behavior of these branching ratios is that $\sigma_{\text{prod}} \times \text{BR}(\rho \rightarrow tt/bb/tb)$ grows with the strength of the direct interactions while $\sigma_{\text{prod}} \times \text{BR}(\rho \rightarrow WW/WZ)$ decreases. Nevertheless, there are particular combinations of the values of $b_{L,R}$ and p when this statement does not hold. For example, if $b_L = 0$ and $p = 0$ the vector resonance decays strongly to tt while it decays to bb only via the indirect interactions not sensitive to these parameters. In such a case, $\text{BR}(\rho \rightarrow tt)$ grows with b_R while $\text{BR}(\rho \rightarrow bb)$ decreases. This very behavior will transfer without alteration into the cross sections of the processes where the neutral resonance is not DY produced. Otherwise, the cross section dependence on the direct interaction parameters will result from the interplay between the BR and production cross section dependences.

In our previous paper [3], we investigated the tBESS mass exclusion limits for the no direct interactions case. In this analysis, all sea partonic quarks, including the b quarks, were ignored. It was a well-justified assumption for the case. Nevertheless, in the paper, we also commented on our expectation regarding the exclusion limits for the case with the direct interactions. Neglecting the b quarks, we expected that the direct interactions would lower the cross sections for the WW/WZ channels and increase the cross sections for the $tt, bb/tb$ channels. Since the latter channels did not reach the experimental upper limits for any admissible values of

$b_{L,R}, p$, we predicted that the presence of the direct interactions would relax the mass exclusion limits. Now, we understand that the bottom quark contribution to the vector resonance production can be ignored only for particular selections of the direct interaction parameters. Thus, our expectation was not correct except for these particular cases.

4 The exclusion limits on the vector resonance mass

In this Section, we work out the mass exclusion limits for the vector triplet of our model by the confrontation of its cross sections (27) with the experimental upper bounds provided by the ATLAS and CMS Collaborations. The regions of the parameter space where the predicted cross section exceeds the upper bounds are excluded. We review fourteen vector resonance decay channels available to the date of this analysis: WZ [12–15], WW [12, 14, 16], WH [12, 17], ZH [12, 17], jj [18, 19], $\ell\ell$ [20], $\ell\nu$ [21], $\tau\tau$ [22], $\tau\nu$ [23], tt [24], bb [25], and tb [26, 27], where $\ell = e, \mu$. The corresponding bounds used in this Section are based on the integrated luminosity of about 36 fb^{-1} (full 2016 data) or less. As was discussed in previous Sections, various experimental and theoretical considerations restrict our mass exclusion limit searches to the following region of the parameter space: $1 \leq M_\rho/\text{TeV} \leq 3$, $12 \leq g'' \leq 25$, $|b_{L,R}| \leq 0.1$, $0 \leq p \leq 1$.

After the analysis advertised above has been finalized new experimental upper bounds have been published by the ATLAS and CMS Collaborations. Some of them were still based on the 36 fb^{-1} [28, 29] dataset, other stemmed from the bigger $77 - 80 \text{ fb}^{-1}$ [30, 31] and 139 fb^{-1} [32–34] datasets. At the end of this Section we append an update on how these new upper bound affect our mass exclusion limits. Nevertheless, since the analysis of all collected LHC data by the Collaborations is still in progress, even these updates of the mass limits can become obsolete in the near future. Yet, we believe that the presented work provide valuable experience independent of the actual values of the mass exclusion limits.

4.1 No direct interactions

The no direct interactions case was already analyzed in our previous work [3]. Out of all inspected channels there, only the WW and WZ channels provided the exclusion limits for the vector resonance mass.

In this paper, the mass exclusion limits based on the updated upper bounds are presented. Besides the

channels considered in [3], a new decay channel, the $\tau\nu$ one [29], has also been added to the current study. The distinction of the DY and VBF production modes for the WW/WZ upper bounds is another novelty. Finally, the proton partonic contents includes the s , c , and b quarks in the calculation of the model's cross section. All these updates have not altered the conclusion of the previous paper [3] that the WW and WZ channels are the only channels providing the mass exclusion limits for the tBESS vector triplet with no direct interactions. Of course, the limits themselves have been changed by this analysis upgrade.

Taking into account the separate upper bounds for both production modes of the WW and WZ channels, our exclusion limits are based on the following six processes: a) the DY production of WW and WZ , b) the VBF production of WW and WZ , and c) the DY+VBF production of WW and WZ . In Fig. 8, the tBESS cross sections for all these modes as functions of M_ρ are shown at $g'' = 12, 16, 20$, and 24 . In addition, the applicable experimental upper bounds from the six channels mentioned above are superimposed on the graphs. The mass regions where the predicted cross section exceeds the experimental upper bound are experimentally excluded.

To avoid the cluttering of the Fig. 8 graphs with unnecessary curves, only the most restricting experimental upper bounds are displayed there. In the WZ_{DY} , WW_{DY} , and WW_{VBF} graphs, the most restricting bounds are provided by a single curve. In the remaining cases, the most restrictive upper bounds are comprised of two curves, each providing the most restrictive bound for a different subregion of the considered resonance mass interval of 1 – 3 TeV. The sources of the displayed upper bound curves of the individual channels are summarized in Table 1. The table also indicates the particular final states that were used to obtain the bounds.

In the tBESS model, the neutral and charged vector resonances are virtually degenerate in mass. Therefore, the exclusion limit is obtained as the higher one of the charge and neutral limits. In particular, we take the most stringent of the limits found in all six processes displayed in Fig. 8. Of course, we can also establish the exclusion limits for individual charge modes independently of each other. The lessons learned from the tBESS vector triplet model can be applied to many other models with similar phenomenological traits.

The tBESS exclusion mass limits for different values of g'' within $14 \leq g'' \leq 25$ are listed in Table 2. The exclusion limits for g'' values below 14 are not shown because their fatness exceeds 40% which makes the limits obtained via the NWA calculations unreliable.

Table 1 The sources of the experimental upper bounds for the WW and WZ channels depicted in Fig 8. Beside the decay channel, the first column also indicates whether the considered production proceeds via the DY production, the VBF production or both. The second column shows what is the integrated luminosity of the data sample used to derive the bound. The third column indicates the final states through which the given channel was observed. The bounds were provided by the ATLAS and CMS Collaborations in the papers referred to in the last column.

channel	luminosity fb^{-1}	final state	reference
WZ_{DY}	36.1	$qqqq + \nu\nu qq + \ell\nu qq + \ell\ell qq + \ell\ell\nu$	[12]
WZ_{VBF}	36.1	$\nu\nu qq + \ell\nu qq + \ell\ell qq + \ell\ell\nu$	[12]
WZ	36.1	$\ell\ell qq + \nu\nu qq$	[13]
	35.9	jj	[14]
	13.2	$\ell\ell qq$	[15]
WW_{DY}	36.1	$qqqq + \ell\nu qq + \ell\nu\ell\nu$	[12]
WW_{VBF}	36.1	$\ell\nu qq + \ell\nu\ell\nu$	[12]
WW	35.9	jj	[14]
	13.2	$\ell\nu qq$	[16]

4.2 The direct interactions included

In this paper, the impact of the direct interactions on the tBESS vector triplet mass exclusion limits is studied for the first time. The direct interactions can affect the limits by increasing the cross sections of the top and bottom quark decay channel processes. It remains to be seen if the increase is sufficient for the cross sections to reach the experimental upper bounds, in some regions of the parameter space at least. Certainly, the direct interactions also affect the cross sections of the W and Z decay channel processes. Thus, the mass exclusion limits will be influenced by the direct interactions even if the top and bottom quark processes fail in providing additional restrictions.

The current upper bounds based on the data from the remaining channels — with leptons, light quarks, and the Higgs boson — are too weak to modify the tBESS triplet mass exclusion limits. Even though the introduction of the direct couplings does affect the tBESS cross sections of these channels, their values remain far below their upper bounds. They also cannot compete with the $tt/bb/tb$ cross sections once the strength of the direct interactions exceeds the level of $|b_{L,R}| \geq 0.02 - 0.03$. Therefore these channels are not able to contribute to the tBESS mass exclusion limits at the current amounts of the collected data. We are not going to further discuss these channels in this paper.

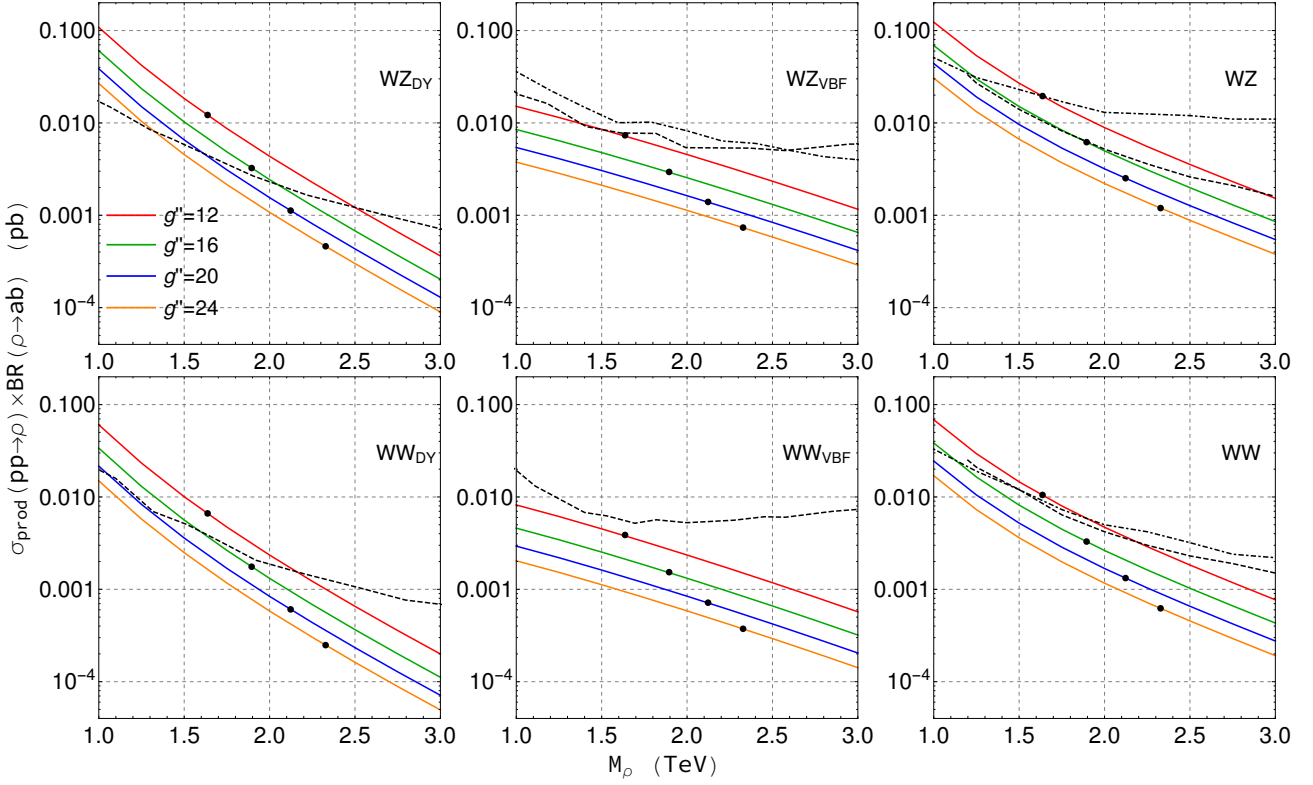


Fig. 8 The plots of $\sigma_{\text{prod}} \times \text{BR}$ predicted by the tBESS model for the WW and WZ channels (solid lines) along with the relevant experimental upper bounds (dashed and dot-dashed lines) as functions of M_ρ assuming no direct interactions of the vector triplet with the top and bottom quarks. The predicted cross sections are shown for four different values of g'' : 12 (red), 16 (green), 20 (blue), 24 (orange). They decrease with g'' . The black dots indicate the resonance mass at which the resonance fatness amounts to 10%. The first row of the graphs correspond to the WZ final state, the second one to the WW final state. The first, second and third columns of the graphs correspond to the DY production, the VBF production and the combination of both, respectively. In all graphs, the 13 TeV proton-proton collisions are considered.

Table 2 The mass exclusion limits (MEL) for the tBESS vector resonance triplet without direct interactions for various values of g'' . The second row contains the values of the resonance fatness. All MEL values shown in the table indicate the upper boundaries of the mass exclusion region.

g''	14	15	16	17	18	19	20	21	22	23	24	25
$\Gamma_{\text{tot}}/M_\rho$	0.39	0.21	0.14	0.10	0.07	0.05	0.03	0.02	0.02	0.01	0.01	< 0.01
MEL (TeV)	2.50	2.21	2.07	1.95	1.83	1.70	1.60	1.51	1.43	1.37	1.31	1.24

tb, tt, bb

The tb channel cross section does not provide the mass exclusion limits for any considered values of the model parameters. In this channel, the sensitivity to the direct interactions enters via the $\text{BR}(\rho \rightarrow tb)$. With the growing strength of the direct interactions, the branching ratio also grows, reaching the limiting value of 1 as $(b_L^2 + p^2 b_R^2) \rightarrow \infty$. Note, however, that there are regions of the parameter space where $\text{BR}(\rho \rightarrow tb)$ exceeds 90% already at $|b_{L,R}| = 0.1$ (see Figs. 3 and 5). In principle, $\sigma_{\text{prod}} \times \text{BR}(\rho \rightarrow tb)$ can assume any value between the no direct interaction cross section and the production cross section if the suppressing Death Valley

region of the parameter space is ignored. In Fig. 9, the plots of these two extremes of the tBESS cross sections as functions of M_ρ for various g'' are shown along with the most restricting experimental upper bounds for this channel. It demonstrates that the current experimental bounds do not exclude the production cross section values. In addition, the estimated upper bound, when the integrated luminosity reaches 3000 fb^{-1} (HL-LHC), is also plotted in the graph⁵. It seems that the 3000 fb^{-1} luminosity will be needed to restrict the vector resonance mass from the data in this channel.

⁵ The hypothetical HL-LHC bound is obtained by a simple rescaling of the current 35.9 fb^{-1} bound by the factor of $\sqrt{35.9/3000}$.

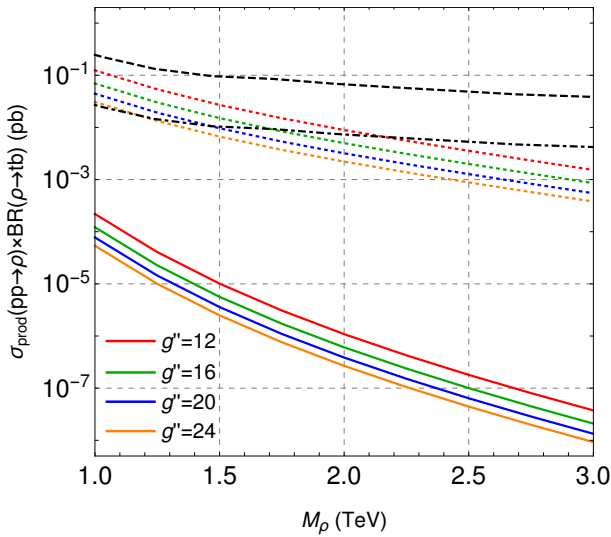


Fig. 9 The plots of $\sigma_{\text{prod}} \times \text{BR}$ predicted by the tBESS model for the tb channel when there are no direct interactions (colored solid lines) and when $\text{BR}(\rho \rightarrow tb) = 1$ (colored dotted lines) along with the relevant experimental upper bounds (black dashed line) as functions of M_ρ . The black dot-dashed line depicts the expected upper bound for the integrated luminosity 3000 fb^{-1} . The predicted cross sections are shown for four different values of g'' : 12 (red), 16 (green), 20 (blue), 24 (orange). They decrease with g'' . The 13 TeV collisions of protons are assumed.

As far as the $t\bar{t}$ and $b\bar{b}$ channels are concerned, they are sensitive to the direct interactions through the $b\bar{b} \rightarrow \rho^0$ production, as well as the vector resonance decays to $t\bar{t}$ and $b\bar{b}$. Nevertheless, in these channels, no mass exclusion limits for the parameter space region under consideration are implied by the current experimental data. The list of the currently most restricting upper bounds, this conclusion is based upon, is shown in Table 3.

Table 3 The sources of the experimental upper bounds for the $t\bar{t}$, $b\bar{b}$, and tb channels we use in our analysis.

channel	luminosity	final state	reference
$t\bar{t}$	35.9 fb^{-1}	dileptons+lepton +hadronic	[24]
$b\bar{b}$	36.1 fb^{-1}	2- b jets	[25]
tb	36.1 fb^{-1}	semileptonic +hadronic	[26]

WW, WZ

In the no direct interaction case, the WW and WZ channels provided the only mass exclusion limits for the tBESS vector triplet. Once the direct interactions

are introduced, the predicted cross section gets modified and become dependent on the values of $b_{L,R}$ and p . The WZ_{DY} , WZ_{VBF} , $WZ_{\text{DY+VBF}}$, and WW_{VBF} cross sections diminish in comparison with the no direct interaction case for all parameter values under consideration. It is because these cross sections depend on $b_{L,R}$ and p through $\text{BR}(\rho \rightarrow WW)$ and $\text{BR}(\rho \rightarrow WZ)$ only.

The behavior of the WW_{DY} cross section is not so easy to conjecture. Its sensitivity to the direct interactions originates not only in $\text{BR}(\rho \rightarrow WW)$ but also in the production of ρ through the $b\bar{b}$ annihilation. Of course, this feature impacts the exclusion limits obtained from the combined (DY+VBF) WW cross section.

When $|b_{L,R}| \leq 0.1$ the cross sections for all three WZ modes lie in the bands between the no direct interaction cross section (the upper boundary) and the $b_L = -b_R = -0.1$ and $p = 1$ cross section (the lower boundary)⁶. The upper boundary of the cross section stripe for the WW_{VBF} mode is also determined by the no direct interaction cross section. The lower boundary is given by the cross section at $b_L = b_R = -0.1$ and $p = 1$.

Regarding the WW_{DY} and $WW_{\text{DY+VBF}}$ modes, their cross sections can either grow or decrease with the growing strength of the direct interactions, depending on the particular combination of the $(b_{L,R}, p)$ parameter values. This more complex behavior originates from the competition between the growing production cross section and the shrinking branching ratio. We determined numerically that when $|b_{L,R}| \leq 0.1$ the WW_{DY} and $WW_{\text{DY+VBF}}$ cross sections are bound from below by the cross section for $b_L = 0, b_R = -0.1, p = 0$. From above, they are bound by the $b_L = -b_R = -0.1$ and $p = 1$ cross section. This behavior is illustrated in Fig. 10 where the bands of possible values of the WW and WZ cross sections as functions of M_ρ , when $|b_{L,R}| \leq 0.1$ and $0 \leq p \leq 1$, are depicted. The bands are constructed for two values of g'' , namely 16 and 20. In addition, the same experimental upper bounds, as in Fig. 8, are superimposed. We can see that the WW_{VBF} and WZ_{VBF} provide no mass exclusion limits for the vector triplet of our model, while the remaining modes do.

Since there are too many free parameters involved, and the behavior of some modes is not simple, it is not possible to find a way to present the mass exclusion limits in a concise manner. Nevertheless, the graphs in Fig. 10 provide information about certain aspects of the mass exclusion limit behavior: whether there are any

⁶ The $WZ_{\text{DY,VBF,DY+VBF}}$ and WW_{VBF} cross sections for all combinations of $b_{L,R}$ values such that $|b_{L,R}| = 0.1$ and $p = 1$ are virtually identical.

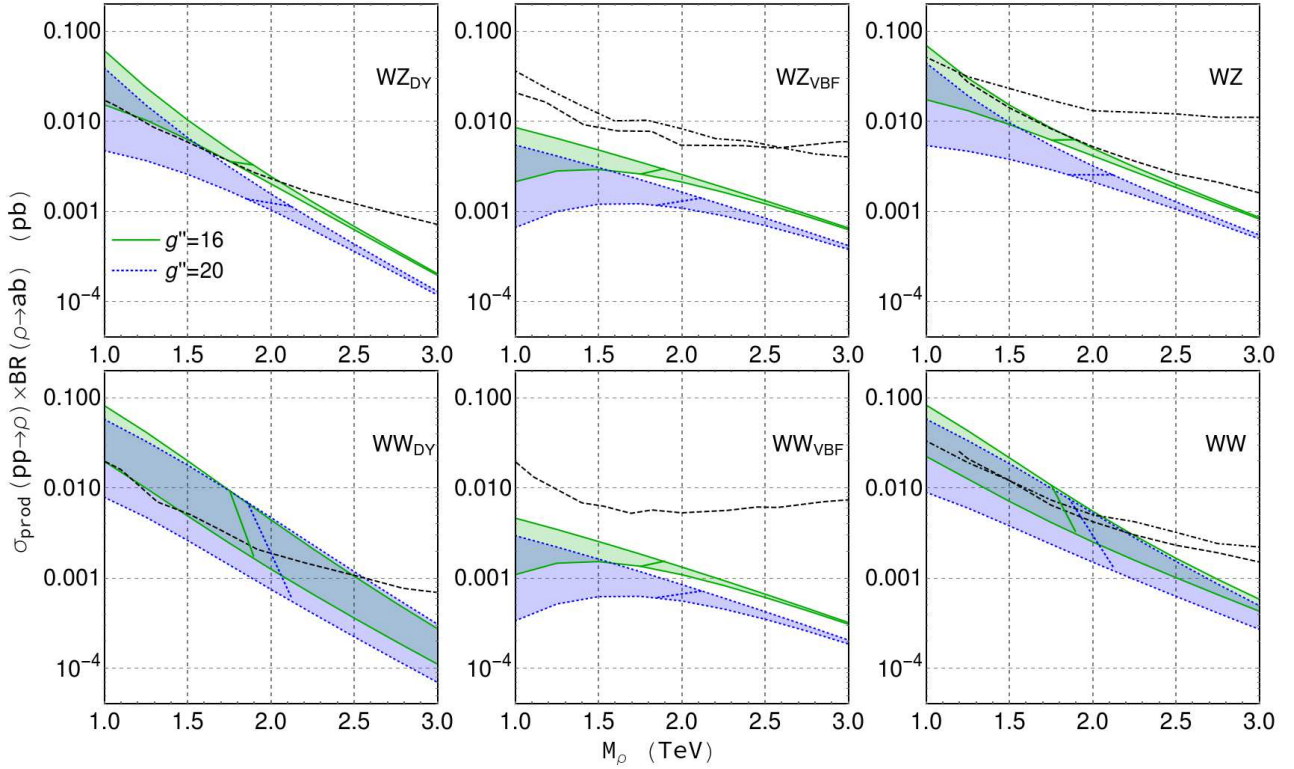


Fig. 10 The bands of possible values of $\sigma_{\text{prod}} \times \text{BR}$ predicted by the tBESS model for the WW and WZ channels produced via the DY, VBF and DY+VBF production modes. The bands are constructed for $g'' = 16$ (solid green) and $g'' = 20$ (dotted blue) when the direct interaction parameters are restricted to $|b_{L,R}| \leq 0.1$ and $0 \leq p \leq 1$. The bands are crossed by the lines of the same style as the bands' boundaries indicating the resonance mass at which the resonance fatness amounts to 10%. The same experimental upper bounds (dashed and dot-dashed black lines) as in Fig. 8 are also shown. In all graphs, the 13 TeV proton-proton collisions are considered.

limits at all, what is the range of their possible values, and so on.

If additional restrictions on the free parameters were imposed more specific information about the exclusion limits could be obtained. For example, let us reduce the number of free parameters of the tBESS model by assuming that $b_L = b_R$ and $p = 1$. It means that the direct interactions are parameterized by a single free parameter $b \equiv b_L = b_R$. In Tab. 4, the smallest mass exclusion limits that can be found from the current WW and WZ experimental upper bounds for various values of g'' when $|b| \leq 0.1$ are shown. The table also displays the value of b and the value of the resonance fatness $\Gamma_{\text{tot}}/M_\rho$ that corresponds to the found mass exclusion limit.

The second reduction of the tBESS model we analyze here is defined by $b_L = 0$ and $b_R = 0.1$. That describes the situation when there are no direct interactions of the vector resonance to the left top and left bottom quarks. The interaction with the right top quark is at the maximum considered in this paper and the interaction with the right bottom quark can be weakened by the only remaining free parameter p . In Tab. 5,

we show the smallest mass exclusion limits that can be found from the current WW/WZ experimental upper bounds for various values of g'' when $0 \leq p \leq 1$. In the table, we also show the value of p and the value of the resonance fatness $\Gamma_{\text{tot}}/M_\rho$ that correspond to the found mass exclusion limit. Note that the used experimental upper bounds provide no mass exclusion limits for $g'' \geq 21$.

To achieve a better understanding of this complex multi-parameter situation we can plot the regions of the (b_L, b_R) parameter subspace for which a certain resonance mass is excluded by the experimental upper bounds when the values of g'' and p are also fixed. As an example, we choose $M_\rho = 1.8$ TeV, $g'' = 18$ and $p = 0.8$. With this choice of the parameters the resonance fatness amounts to $\Gamma_{\text{tot}}/M_\rho = 6\%$ at $b_L = b_R = 0$. As both, $|b_L|$ and $|b_R|$ approach 0.1 the fatness grows to 9%. Thus we can expect that the deviations introduced by the NWA calculations are reasonably small. The resulting plot of the experimentally excluded regions in the (b_L, b_R) space is shown in Fig. 11. The excluded region is obtained by the union of the areas excluded by the WZ_{DY} and WW_{DY} decay channels.

Table 4 The smallest tBESS resonance mass exclusion limits (MEL) within the interval $|b_{L=R}| \leq 1$ assuming $b_{L=R} \equiv b_L = b_R$ and $p = 1$ for various values of g'' . The second and third rows contain, respectively, the values of $b_{L=R}$ and of the resonance fatness $\Gamma_{\text{tot}}/M_\rho$ that correspond to the quoted mass exclusion limit. The excluded masses lie below MEL.

g''	14	15	16	17	18	19	20	21	22	23	24	25
$b_{L=R} \times 10^2$	9.5	5.6	4.4	3.6	3.2	2.8	2.5	2.0	1.7	1.7	1.7	1.6
$\Gamma_{\text{tot}}/M_\rho$	0.36	0.20	0.14	0.10	0.06	0.04	0.03	0.02	0.02	0.01	≤ 0.01	≤ 0.01
MEL (TeV)	2.42	2.15	2.04	1.92	1.77	1.64	1.53	1.44	1.38	1.30	1.11	1.03

Table 5 The smallest tBESS resonance mass exclusion limits (MEL) within the interval $0 \leq p \leq 1$ assuming $b_L = 0$ and $b_R = 0.1$ for various values of g'' . The second and third rows contain, respectively, the values of p and of the resonance fatness that correspond to the quoted mass exclusion limit. The excluded masses lie below MEL.

g''	14	15	16	17	18	19	20	21 – 25
p	1	0.871	0.772	0.707	0.672	0.630	0.589	–
$\Gamma_{\text{tot}}/M_\rho$	0.38	0.20	0.14	0.09	0.06	0.04	0.03	–
MEL (TeV)	2.46	2.14	2.02	1.87	1.68	1.49	1.33	no MEL

The ring-like structure depicted in Fig. 11 can be understood from the no-direct-interaction graphs of Fig. 8 and from their response to the direct interactions being turned on. With no direct interactions, the only channel that excludes the 1.8 TeV vector triplet is the WZ_{DY} one. However, the tBESS cross section of this channel decreases with the direct interactions strength. When the direct interactions become sufficiently strong the predicted value dives below the experimental one and the channel ceases to exclude the resonance. On the other hand, owing to the partonic bottom quark contribution, the WW_{DY} decay channel cross section grows with the direct interaction strength. When the direct interactions are turned off the resonance is not excluded by the channel. However, its predicted cross section exceeds the measured value when the direct interactions become sufficiently strong and, thus, excludes the given resonance. Since the exclusion boundary of the WZ_{DY} channel are closer to the origin $b_L = b_R = 0$ than the exclusion boundary of the WW_{DY} channel a ring-like region of the (b_L, b_R) parameter subspace, where the resonance is not excluded, has emerged. The resonance fatness at the WW_{DY} boundary is 7%.

The excluded region shown in Fig. 11 is very sensitive to the values of the resonance mass. This is demonstrated in Fig. 12. The figure consists of the graphs which show the excluded regions of the (b_L, b_R) subspace for the values of M_ρ that slightly vary around the mass considered at the graph of Fig. 11. The excluded regions change significantly even within the small range $1.75 \leq M_\rho/\text{TeV} \leq 1.85$ for all three chosen values of $p = 0.4, 0.7, 1$. We suggest that the combination of this feature and the sufficiently large imprecision caused by any used approximation can result in a quite deceiving conclusions about the exclusion of the resonance of

a given mass. Thus, the deviations introduced by the NWA calculations should be carefully scrutinized as the fatness of the resonance under consideration grows.

It seems obvious that an exhaustive study of the experimentally excluded areas of the complete tBESS parameter space would be a cumbersome task even though the tBESS phenomenological Lagrangian corresponds to a relatively simplistic LHC scenario. The real scenario of the strongly-interacting extension of the SM can introduce even more complex phenomenology of the new resonances to be discovered at the LHC. Even if this is the case the tBESS model analysis can provide valuable lessons. While any simplifying assumptions that would help with the detection analysis are certainly appreciated, one has to remember that this can come at the price of losing sensitivity to more subtle behavior of the studied resonances.

4.3 An experimental update

In this subsection, we provide a brief review on how the recently published experimental upper bounds on $\sigma_{\text{prod}} \times \text{BR}$ changed the mass exclusion limits calculated above. These latest upper bounds originate from the ongoing analyses of the data collected at the LHC experiments. While there have been about 139 fb^{-1} of data recorded to the date the progress of their analysis lags behind. There are still new bounds being published that are even based on the 2016 dataset of 36 fb^{-1} .

As expected, even with the bigger integrated luminosity the WW and WZ are the only channels that provide restrictions on the tBESS production cross sections. In particular, the new upper bounds for the WZ channel were published in [28] and [34]. The upper bounds

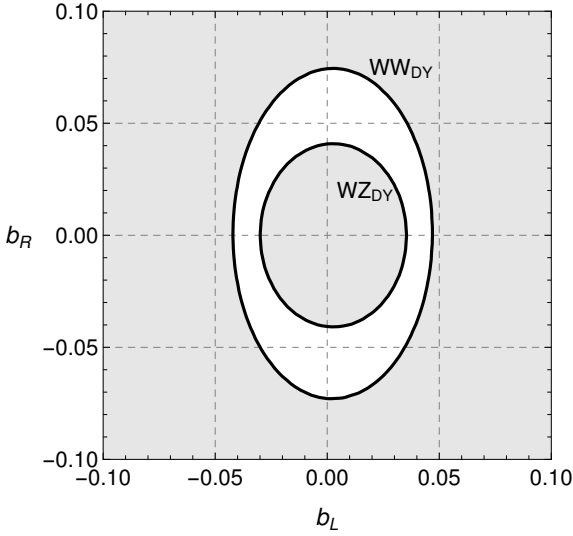


Fig. 11 The excluded region of the (b_L, b_R) -plane (gray area) for the vector resonance with the mass of $M = 1.8$ TeV, $g'' = 18$, $p = 0.8$.

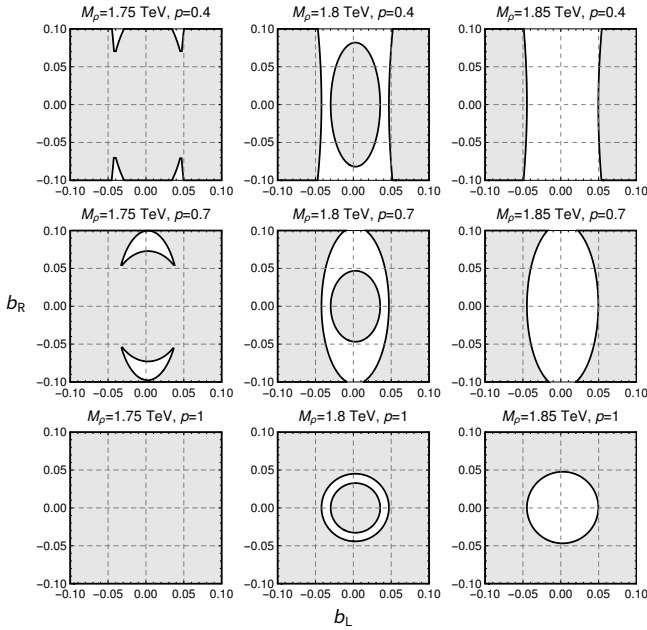


Fig. 12 The grid of graphs of the excluded regions of the (b_L, b_R) -plane (gray area) when $g'' = 18$. The mass changes from graph to graph in the left-to-right direction through the values of 1.75, 1.80, and 1.85 TeV. The p parameter changes from the top to the bottom through the values of 0.4, 0.7, and 1.0.

were based on the 36 fb^{-1} and 139 fb^{-1} datasets, respectively. The new upper bounds for the WW channel were published in [30] and [34]. The upper limits of the former paper were based on the 77 fb^{-1} dataset. The new bounds in [34] apply to the mass range above 1.3 TeV only. In combination with some of the previous upper bounds [16], these new experimental bounds re-

sult in new mass exclusion limits for the tBESS vector triplet.

To demonstrate the effect of the new upper bounds we update the mass exclusion limits for the scenarios presented in Tables 2, 4, and 5. Thus, Table 6 contains the updated mass exclusion limits when there are no direct interactions. The updated values for the scenarios of Tables 4 and 5 are shown in Tables 7 and 8, respectively. We can see that the mass exclusion limits have increased by more than 1 TeV. In addition, all corresponding fatnesses have surpassed the 10% mark which makes the presented conclusions less reliable. That is why we restrain ourselves from displaying the mass exclusion limits when they exceed 3 TeV where the precision of the NWA calculations becomes very questionable.

5 Conclusions

Motivated by the absence of any signal of new particles beyond the SM in the LHC measurements, we have studied the mass exclusion limits for the hypothetical tBESS vector resonance triplet. The exclusion limits have been established utilizing the experimental upper bounds on the s -channel resonance production cross section times branching ratio provided by the ATLAS and CMS Collaborations for various decay channels.

The tBESS resonance triplet represents a possible signature of a strongly-interacting extension of the SM. It has been introduced in the context of the phenomenological Lagrangian where, besides the composite 125 GeV Higgs boson, the $SU(2)_{L+R}$ triplet of composite vector resonances is explicitly present. The vector resonance has been built into the Lagrangian employing the hidden local symmetry approach. In the tBESS model, the vector triplet interacts universally with all fermions due to the mixing between the electroweak gauge boson fields and the vector triplet. In addition, the direct couplings of the vector triplet to the top and bottom quarks have been introduced.

Fourteen vector resonance decay channels, for which the experimental upper bounds were available to the date, have been considered in our analysis. Of these, only the WW and WZ channels provide the mass exclusion limits for the tBESS vector triplet in both direct interaction scenarios.

The impact of the direct interactions on the mass exclusion limits has been contrasted with the no direct interaction case. As expected, the introduction of the specific direct interaction pattern to the model has made the analysis of the limits significantly more complex. Besides the emergence of new free parameters,

Table 6 The updated mass exclusion limits (MEL) for the tBESS vector resonance triplet without the direct interactions for various values of g'' .

g''	12 – 20	21	22	23	24	25
$\Gamma_{\text{tot}}/M_\rho$	> 0.40	0.33	0.26	0.21	0.17	0.13
MEL (TeV)	> 3	2.94	2.84	2.73	2.65	2.53 ^a

^a the mass is also not excluded within (1.24; 1.30) TeV

Table 7 The updated smallest tBESS resonance mass exclusion limits (MEL) within the interval $|b_{L=R}| \leq 1$ assuming $b_{L=R} \equiv b_L = b_R$ and $p = 1$ for various values of g'' . The second and third rows contain, respectively, the values of $b_{L=R}$ and of the resonance fatness $\Gamma_{\text{tot}}/M_\rho$ that correspond to the quoted mass exclusion limit.

g''	12 – 19	20	21	22	23	24	25
$b_{L=R} \times 10^2$		8.6	7.6	6.7	5.9	4.8	4.0
$\Gamma_{\text{tot}}/M_\rho$	> 0.44	0.41	0.32	0.25	0.20	0.15	0.12
MEL (TeV)	> 3	2.96	2.86	2.74	2.65	2.52 ^a	2.41 ^b

^a the mass is also not excluded within (1.11; 1.30) TeV

^b the mass is also not excluded within (1.03; 1.30) TeV

Table 8 The updated smallest tBESS resonance mass exclusion limits (MEL) within the interval $0 \leq p \leq 1$ assuming $b_L = 0$ and $b_R = 0.1$ for various values of g'' . The second and third rows contain, respectively, the values of p and of the resonance fatness that correspond to the quoted mass exclusion limit.

g''	12 – 19	20	21	22	23	24	25
p		1	1	0.962	0.910	0.796	0.755
$\Gamma_{\text{tot}}/M_\rho$	> 0.44	0.40	0.32	0.25	0.20	0.14	0.11
MEL (TeV)	> 3	2.97	2.87	2.73	2.63	2.45	2.28

the direct interactions have made the bottom quark partonic content of the proton significant for the neutral resonance production in the Drell-Yan mode. In fact, there are the parameter space regions where over 90% of the neutral resonance production is comprised of $b\bar{b} \rightarrow \rho^0$. Consequently, the sensitivity of $b\bar{b} \rightarrow \rho^0$ to the direct interaction couplings impacts all mass exclusion limits founded on the neutral resonance channels including the WW one. The disregard of the bottom quark contents of the colliding protons would alter our results qualitatively. The contribution of the partonic charm and strange quarks to the neutral and charged vector resonance production is about 5 – 7%.

The experimental upper bounds used in our analysis were derived with the narrow resonance qualification. Consistently, the model cross section predictions have been calculated in the narrow width approximation. As a rule of thumb we consider our analysis as reliable for the resonance fatness below 10%. The results obtained for the resonances with the fatness above this mark must be considered with caution. This is an important issue in the case of the tBESS vector resonance triplet whose decay width grows significantly with its mass.

When there are no direct interactions the resonance mass exclusion limits range between 2.94 TeV and 2.53 TeV for g'' between 21 and 25, respectively. The respective

resonance fatnesses range between 33% and 13%. Unfortunately, these are already above the 10% rule of thumb. Thus, the quoted limits should be considered with caution. When $g'' \leq 20$ the mass exclusions limit exceeds 3 TeV and the corresponding fatness surpasses 40%. Therefore, we do not even attempt to quote the particular exclusion limits obtained by the NWA calculations for $g'' \leq 20$.

For the scenario with the direct interactions, the mass exclusion limits for two different sets of the parameter constraints have been studied. First, it has been assumed that the direct interactions are L-R and top-bottom universal, i.e., $b_L = b_R$, $p = 1$. In the second case, it has been assumed that there are no direct interactions to the left top-bottom quark doublet ($b_L = 0$) and that the resonance couples strongly to the right top-bottom quark doublet ($b_R = 0.1$). The relative strength of the direct interactions to the top and bottom quark has been left as a free parameter. In both cases, the minimal mass exclusion limits, when varying the remaining free parameters, have been found. In the first case, the limit ranges from 2.96 TeV to 2.41 TeV for $g'' = 20$ and $g'' = 25$, respectively. The respective resonance fatnesses range between 41% and 12%. In the second case, the mass exclusion limits for g'' between 20 and 25 range from 2.97 TeV to 2.28 TeV, respectively.

The respective resonance fatnesses range between 40% and 11%. In both cases, the mass exclusion limits exceed 3 TeV when $g'' \leq 19$. The corresponding resonance fatnesses surpass 44%.

Acknowledgements The work was supported by the grant LTT17018 of the Ministry of Education, Youth and Sports of the Czech Republic. M.G. was supported by the Slovak CERN Fund. We would also like to thank the Slovak Institute for Basic Research for their support.

References

1. M. Bando, T. Kugo, and K. Yamawaki, *Phys. Rep.* **164**, 217 (1988).
2. R.S. Chivukula et al, *Phys. Rev. D* **74**, 075011 (2006).
3. M. Gintner, J. Juráň, *Acta Physica Polonica B* **48**, 1383 (2017); arXiv: 1705.04806.
4. M. Gintner, J. Juráň, and I. Melo, *Phys. Rev. D* **84**, 035013 (2011).
5. M. Gintner, J. Juráň, *Eur. Phys. J. C* **73**, 2577 (2013).
6. M. Gintner, J. Juráň, *Eur. Phys. J. C* **76**, 651 (2016), erratum, *Eur. Phys. J. C* **77**, 6 (2017); arXiv: 1608.00463.
7. R. Casalbuoni, S. De Curtis, D. Dominici, and R. Gatto, *Phys. Lett.* **155B**, 95 (1985); *Nucl. Phys.* **B282**, 235 (1987); R. Casalbuoni, P. Chiappetta, S. De Curtis, F. Feruglio, R. Gatto, B. Mele, and J. Terron, *Phys. Lett.* **B249**, 130 (1990).
8. D. Pappadopulo, A. Thamm, R. Torre and A. Wulzer, *JHEP* 1409 (2014) 060.
9. S. Dawson, *Nucl. Phys.* **B249**, 42 (1985).
10. D.B. Clark, E. Godat, F.I. Olness, arXiv:1605.08012. Mane Parse package download: <https://ncteq.hepforge.org/mma/index.html>
11. A. Buckley et al., *Eur. Phys. J. C* **75**, 132 (2015); arXiv:1412.7420. LHAPDF6 PDFs download: <http://lhapdf.hepforge.org/pdfsets>
12. ATLAS Collaboration, ATLAS-CONF-EXOT-2017-31.
13. ATLAS Collaboration, *JHEP* 03 (2018) 009; arXiv:1708.09638.
14. CMS Collaboration, CMS-PAS-B2G-17-001.
15. ATLAS Collaboration, ATLAS-CONF-2016-082.
16. ATLAS Collaboration, ATLAS-CONF-2016-062.
17. ATLAS Collaboration, *JHEP* 03 (2018) 174; arXiv:1712.06518.
18. *Phys. Rev. D* **96**, 052004 (2017); arXiv:1703.09127.
19. CMS Collaboration, CMS-PAS-EXO-16-056.
20. ATLAS Collaboration, ATLAS-CONF-2017-027.
21. ATLAS Collaboration, ATLAS-CONF-2017-016.
22. ATLAS Collaboration, *JHEP* 01 (2018) 055; arXiv:1709.07242.
23. ATLAS Collaboration, *Phys. Rev. Lett.* **120**, 161802 (2018); arXiv:1801.06992.
24. CMS Collaboration, *JHEP* 04 (2019) 031; arXiv:1810.05905.
25. ATLAS Collaboration, *Phys. Rev. D* **98**, 032016 (2018); arXiv:1805.09299.
26. ATLAS Collaboration, *Phys. Lett.* **B788**, 347 (2019); arXiv:1807.10473.
27. CMS Collaboration, CMS-PAS-B2G-17-010.
28. CMS Collaboration, CMS-PAS-B2G-18-006.
29. CMS Collaboration, *Phys. Lett.* **B792**, 107 (2019); arXiv:1807.11421.
30. CMS Collaboration, CMS-PAS-B2G-18-002.
31. ATLAS Collaboration, ATLAS-CONF-2018-017.
32. ATLAS Collaboration, ATLAS-CONF-2019-007.
33. ATLAS Collaboration, ATLAS-CONF-2019-001.
34. ATLAS Collaboration, ATLAS-CONF-2019-003.